Computational Mechanics (2022) 70:803–818
https://doi.org/10.1007/s00466-022-02209-3

ORIGINAL PAPER

Phase-field approach to evolution and interaction of twins in single crystal magnesium

Benhour Amirian[1] · Hossein Jafarzadeh[2] · Bilen Emek Abali[3] · Alessandro Reali[2] · James David Hogan[1]

Received: 6 March 2022 / Accepted: 23 June 2022 / Published online: 27 July 2022

Abstract
Crack initiation and propagation as well as abrupt occurrence of twinning are challenging fracture problems where the transient phase-field approach is proven to be useful. Early-stage twinning growth and interactions are in focus herein for a magnesium single crystal at the nanometer length-scale. We demonstrate a basic methodology in order to determine the mobility parameter that steers the kinetics of phase-field propagation. The concept is to use already existing molecular dynamics simulations and analytical solutions in order to set the mobility parameter correctly. In this way, we exercise the model for gaining new insights into growth of twin morphologies, temporally-evolving spatial distribution of the shear stress field in the vicinity of the nanotwin, multi-twin, and twin-defect interactions. Overall, this research addresses gaps in our fundamental understanding of twin growth, while providing motivation for future discoveries in twin evolution and their effect on next-generation material performance and design.

Keywords Phase-field model · Single crystal magnesium · Twinning interactions · Monolithic scheme

1 Introduction

Developing next-generation materials with controlled twinning behaviors offers promising opportunities for improved mechanical properties [1,2] and performance in engineering applications (e.g., gas turbine engines [3] and lightweight automotive structures [4]). Among materials that exhibit twinning [5–8], magnesium [9–12] is an example of a lightweight metal where slip and twinning, as the two main crystallographic mechanisms, play a decisive role in its mechanical response; here, twinning is favorable on pyramidal $\{1012\}\langle 1011\rangle$ systems at room temperature [13]. In magnesium, single twinning occurs through contraction [14] and extension strains [15] along the c-axis [16]. Recent twinning studies have focused on observations of asymmetric twin growth due to heterogeneous grain deformation in the vicinity of the twin [17,18]. We understand that interaction of twin boundaries with other defects (i.e., voids and self-interstitials) increases the likelihood for void nucleation, cracking, and premature failure, leading to degradation of material performance and reduction of material lifetime [19,20]. Recent efforts have also been made to model the twin local stress accurately by means of neighboring grains to accommodate the transformation [21]. In engineering applications, there is a broad interest in incorporating magnesium in high strain-rate applications (e.g., aerospace [22]), where twin growth and evolution limits the mechanical performance [23]. However, knowledge gaps in understanding twin growth [24], thickening [25], and interactions [26] need to be addressed before the adoption of magnesium-based alloys into these applications; these are studied herein for a single crystal Mg material system.

✉ Benhour Amirian
benhour@ualberta.ca

✉ Hossein Jafarzadeh
hossein.jafarzadeh@unipv.it

✉ Bilen Emek Abali
bilenemek@abali.org

Alessandro Reali
alereali@unipv.it

James David Hogan
jdhogan@ualberta.ca

[1] Department of Mechanical Engineering, University of Alberta, Edmonton T6G 2R3, AB, Canada

[2] Department of Civil Engineering and Architecture, University of Pavia, I-27100 Pavia, Italy

[3] Department of Materials Science and Engineering, Uppsala University, 751 21 Uppsala, Sweden

Ample experimental measurements exist on time-resolved twin evolution in magnesium [27]. In situ data is limited effected by the limitations in available diagnostics to capture growth and evolution behaviors at sufficient length and time scales [28]. To this end, atomistic simulations have been widely adopted to probe effects such as atomic shuffling mechanisms for propagation of twins in magnesium [29], disconnections and other defects associated with the twin interface [30], and reaction of lattice dislocations with twin boundaries [31]. While new understandings have been gained to accurately model plastic deformation and fracture in magnesium [32,33], atomistic simulations are limited in their ability to simulate twinning behaviors at relevant length and time scales needed for practical implementation in engineering applications. Challenges also exist in molecular dynamic approaches in applying characterization algorithms (e.g., centrosymmetry parameter [34] and bond angle analysis [35]) to interpret post-deformation crystal structure defect types (e.g., twinning) [36]. Continuum mechanics modeling utilizing crystal plasticity theory is yet another modeling approach for predicting the twinning and de-twinning response in materials with hexagonal close-packed crystal structures [37–39]. However, crystal plasticity modeling has difficulties to capture the twinning process correctly due to treating the twinning deformation as a unidirectional shear deformation mode [40]. Additionally, the conventional crystal plasticity model is unable to investigate the effect of twin microstructure on the mechanical behavior of magnesium at the nanometer scale [41]. Overcoming such limitations, we model herein the twinning process by a phase-field approach where the mobility parameter is determined by an inverse analysis. Such a computational implementation allows us to unravel time-evolved twinning behavior in magnesium.

For the morphological evolution of twins, the mesoscale phase-field model [42–47] has been extensively used to study the nucleation [48], growth [49], and propagation of twinning [50]. Most recent computational approaches to phase field equations for studying deformation twinning in magnesium at the microscale were based on the Fourier spectral method [50–52]. However, such an approach is only applicable to cases involving periodic boundary conditions and for morphologies and microstructures dominated by long-range elastic interactions [53]. Also, spectral method is mostly used for solving linear problems [54]. In [52,55,56], the proposed phase-field simulations for deformation twinning and dislocation induced plasticity in hexagonal closed-pack materials were formulated on small strain theory; still, the twin evolution is usually accompanied by large interface orientation and large shear deformations [57] even under small strains [58]. Thus, coupling between twin evolution and fracture is of importance to achieve high accuracy in the numerical solution. In terms of validating the phase-field results of transmission mechanisms of deformation twins, atomistic simulations (e.g., molecular dynamics simulations [50,55] and density functional theory [52]) and experimental results [51,59] are the most widely used. Some drawbacks to these validations exist such as

- discrepancies of the peak stress value from the simulation and experimental data [51],
- qualitative comparison of distribution of order parameter using the isotropic gradient energy parameter [52,55,56],
- adopting empirically determined large non-physical values for the phase-field parameters (e.g., twin-twin interfacial energy, initial twin nucleus, and energy barrier heights between the matrix and the twinning [50,51]), and
- validating at the different length-scales [50,60].

Hence, the application of their model is somehow limited for studying the deformation mechanisms of Mg. The development of nanoscale phase-field models is therefore required and all the mentioned shortcomings are addressed in this work.

Building on these past works, this current article utilizes a monolithically-solved finite element method for solving an advanced physics-based phase-field approach to study the nanoscale growth of existing twins in anisotropic single crystal magnesium. We follow [61] for modeling the twinning interface propagation kinetics, which is important for the realistic description of twinning deformation. The model sheds light on the growth and evolving of twinning embryo.

A finite size sample with a hole is considered for studying the interactions of twin with defects, without the need of periodic boundaries. We implement nonlinear elasticity coupled to Ginzburg–Landau equations for order parameters. By using a highly nonlinear phase-field approach, we model anisotropic surface energy allowing to simulate large deformation of defect-free volumes at the nanoscale. Motivated by the literature [62–66], we use a mobility parameter and devote the work for determining this value for a specific material, namely single crystal Mg. The time evolution of the twin order parameter is directly proportional to the resolved shear stress. This outcome is useful for modeling deformation twinning since the propagation speed of twin boundaries is difficult to measure experimentally, and could even be supersonic if the driving stress is sufficiently large [67].

We verify the proposed implementation of the time-resolved continuum-based model for magnesium by the static phase-field model [68] and molecular dynamics (MD) simulations [69] (Fig. 1). By choosing the same length-scale for the phase-field model and MD simulations, we assure the compatibility of MD results with our implementation, which is often left aside in the literature [51,56,60]. It is

also worth stating that all MD simulations use extremely high deformation rates, making it difficult to understand whether a phenomenon results from the rate sensitivity of the material or is a numerical artifact [70,71]. To remedy this, various strategies can be used to bridge the gap between the atomic scale and continuum frameworks, such as large-scale MD calculations [72], coarse-graining [73], and ultra-high strain-rate tests [74]. Twin propagation speed is explored (Fig. 2) and compared with MD results [69] and analytical solutions [75]. In this way, we demonstrate a simple yet effective approach on how to determine the mobility parameter. Moreover, insights in growth rates are of interest given the limited available data [27] and studying these behaviors is vital in high-rate applications of magnesium [76]. Our presented results are then validated in terms of twin area fraction and global shear stress (Fig. 3), and the role of twin-twin and twin-defect interactions is explored (Fig. 4). Through these approaches, the research offers broad potential in materials design, and motivates promising directions in experimental and computational materials science.

2 Governing equations

We use standard continuum mechanics notation, where Latin indices refer to spatial coordinates. We use Einstein's summation convention over repeated indices. All tensors are expressed in Cartesian coordinates. The superscripts E and IE stand for elastic (recoverable) and inelastic (irreversible) deformations, respectively. For the description of the twin, an order (phase-field) parameter, η, is introduced, where $\eta = 0$ denotes the parent crystal and $\eta = 1$ means the twin. This order parameter as well as displacement, $\boldsymbol{u}$, are the primitive variables in space and time that we are searching for. The deformation gradient reads

$$F_{ij} = u_{i,j} + \delta_{ij}, \tag{1}$$

where comma denotes a derivative in space. We use a material frame, where the derivative is taken in the reference configuration that is chosen to be the initial placement of the continuum body. Kronecker delta, $\boldsymbol{\delta}$, is the identity. The deformation gradient, $\boldsymbol{F}$, in a large-displacement formulation, is decomposed into elastic and inelastic parts,

$$F_{ij} = F^{\mathrm{E}}_{ik} F^{\mathrm{IE}}_{kj}, \tag{2}$$

where for (inelastic) twinning [77], we use

$$F^{\mathrm{IE}}_{ij} = \delta_{ij} + \phi(\eta)\gamma_0 s_i m_j. \tag{3}$$

The interpolation function, $\phi(\eta) = \eta^2(3-2\eta)$, causes a steep change between the twin and parent crystal [78] as necessary in phase-field approaches. γ_0 is the magnitude of maximum twinning shear, and $\boldsymbol{s}$ and $\boldsymbol{m}$ are the unit vectors along the twinning direction and normal to the twinning plane, respectively. By following [79], we decompose the Helmholtz free energy per mass into mechanical and interfacial parts,

$$\psi(\boldsymbol{F}, \eta, \nabla\eta) = \psi^{\mathrm{M}}(\boldsymbol{F}, \eta) + \psi^{\nabla}(\eta, \nabla\eta)\ , \tag{4}$$

where the kinetics of interface is controlled by twin order parameter and its first-gradient by the latter. As usual, for the mechanical deformation energy density (per volume), we may use the St. Venant model:

$$\rho_0 \psi^{\mathrm{M}} = \frac{1}{2} E_{ij} C_{ijkl} E_{kl}\ , \tag{5}$$

or the neo-Hookean model:

$$\rho_0 \psi^{\mathrm{M}} = \frac{\mu}{2}(I_C - 3) - \mu \ln J + \frac{\lambda}{2}(\ln J)^2\ . \tag{6}$$

For nonlinear isotropic elasticity, the neo-Hookean model defined in Eq. (6) is used. We use right Cauchy–Green deformation tensor, $C^{\mathrm{E}}_{ij} = F^{\mathrm{E}}_{ki} F^{\mathrm{E}}_{kj}$, and its invariants, $I_C = C^{\mathrm{E}}_{ii}$, $J = \det(\boldsymbol{C}^{\mathrm{E}})$. The Green–Lagrange strain measure, $\boldsymbol{E} = \frac{1}{2}(\boldsymbol{C}^{\mathrm{E}} - \boldsymbol{\delta})$, accommodates geometric nonlinearity necessary for some applications herein. Lamé parameters, λ, μ, or the stiffness tensor of rank four, C_{ijkl}, are given as material coefficients. The elastic constants are the Voigt-averaged shear and bulk modulus [80], which are listed in Table 1. For anisotropic elasticity, the elastic coefficients are interpolated between the untwinned C^{P}_{ijkl} and twinned C^{T}_{ijkl} domains using the interpolation function,

$$C_{ijkl} = C^{\mathrm{P}}_{ijkl} + (C^{\mathrm{T}}_{ijkl} - C^{\mathrm{P}}_{ijkl})\phi(\eta)\ . \tag{7}$$

The same interpolation function is used as in the definition of the inelastic part of the deformation gradient. For the twin phase, $\eta = 1$, we have the stiffness tensor as a rotation of crystal lattice from the parent phase, $\eta = 0$, as follows:

$$C^{\mathrm{T}}_{ijkl} = \mathcal{Q}_{im}\mathcal{Q}_{jn}\mathcal{Q}_{ko}\mathcal{Q}_{lp} C^{\mathrm{P}}_{mnop}, \tag{8}$$

where $\mathcal{Q}$ is the reorientation matrix associated with twinning. For a centrosymmetric structure [81], it becomes

$$\mathcal{Q}_{ij} = \begin{cases} 2m_i m_j - \delta_{ij} & \text{type I twins,} \\ 2s_i s_j - \delta_{ij} & \text{type II twins.} \end{cases} \tag{9}$$

In the case of a steady-state deformation and neglecting inertial terms, the governing equations for displacement read

$$\begin{aligned} P_{ji,j} =& 0\,, \\ P_{ji} =& \frac{\partial \rho_0 \psi}{\partial F_{ij}} = \frac{\partial \rho_0 \psi^{\mathrm{M}}}{\partial F_{ij}} = \frac{\partial \rho_0 \psi^{\mathrm{M}}}{\partial E_{kl}} \frac{\partial E_{kl}}{\partial F_{ij}} \\ =& \frac{\partial \rho_0 \psi^{\mathrm{M}}}{\partial E_{kl}} F^{\mathrm{E}}_{il} (\boldsymbol{F}^{\mathrm{IE}})^{-1}_{jk}\,. \end{aligned} \tag{10}$$

The Ginzburg–Landau equation is acquired by a thermodynamically-consistent derivation, as follows:

$$\dot{\eta} = -\mathcal{L}\left(\frac{\partial \rho_0 \psi^{\mathrm{M}}}{\partial \eta} + \frac{\partial \rho_0 \psi^{\nabla}}{\partial \eta} - \left(\frac{\partial \rho_0 \psi^{\nabla}}{\partial \eta_{,i}} \right)_{,i} \right), \tag{11}$$

where the mobility parameter, $\mathcal{L}$, is generally not known and challenging to obtain experimentally. The outcome of this work is the methodology on how to set its numerical value.

The first term is formulated by using the product rule

$$\begin{aligned} \frac{\partial \rho_0 \psi^{\mathrm{M}}}{\partial \eta} &= \frac{\partial \rho_0 \psi^{\mathrm{M}}}{\partial F_{ij}} \frac{\partial F_{ij}}{\partial \eta} = P_{ji} \frac{\partial F^{\mathrm{E}}_{ik} F^{\mathrm{IE}}_{kj}}{\partial \eta} \\ &= P_{ji} F^{\mathrm{E}}_{ik} \phi'(\eta) \gamma_0 s_k m_j\,, \end{aligned} \tag{12}$$

where $\phi'(\eta) = 6\eta(1-\eta)$. For the interfacial energy, ψ^{∇}, we use a standard double-well potential as in [82,83] such that the energy density reads

$$\rho_0 \psi^{\nabla}(\eta) = A\eta^2 (1-\eta)^2 + \kappa_{ij} \eta_{,i} \eta_{,j}, \tag{13}$$

where $A = 12\frac{\Gamma}{l}$ characterizes the energy barrier between two stable phases (minima), related to the twin boundary surface energy, Γ, and the twin boundary thickness, l; $\kappa_{ij} = \kappa_0 \delta_{ij}$ with κ_0 being the gradient energy parameter, given as [68], $\kappa_0 = \frac{3}{4}\Gamma l$. By inserting the energy definitions into the Ginzburg–Landau, we obtain the governing equation for twin order parameter,

$$\begin{aligned} \dot{\eta} =& -\mathcal{L}\Big(P_{ji} F^{\mathrm{E}}_{ik} \phi'(\eta) \gamma_0 s_k m_j + 2A\eta\big(1 - 3\eta + 2\eta^2\big) \\ & -2\kappa_0 \eta_{,ii} \Big) \end{aligned} \tag{14}$$

By solving Eqs. (10), (14), we obtain $\boldsymbol{u}$ and η fields.

3 Computational implementation

The presented numerical simulations employ a monolithic strategy in order to solve Eqs. (10), (14). Because of their inherent coupling, a monolithic solution method is preferable for capturing all effects accurately, especially in extreme loading conditions. Mostly, a staggered scheme is implemented partly to increase efficiency yet also effected by numerical difficulties in implementing as a monolithic strategy. Herein, we use the interface energy as described above, which helps to circumvent any numerical convergence errors in the implementation. In a monolithic scheme, for each time step, displacements and order parameter are solved at once. Therefore, for the space discretization, we use an adequate mixed space formulation in the implementation. Specifically, we use $\boldsymbol{u}$ and η as approximated functions spanned over a triangulation with a compact support. This well-known finite element method (FEM) ensures a monotonic convergence for the implementation. We skip a notational distinction between the analytical functions and their approximations since they never show up together.

The computational domain, Ω, is the continuum body's image in the physical space. The domain, Ω, and its closure as a Lipschitz boundary, $\partial\Omega$, form a continuous domain without singularities. Therefore, all form functions are continuous as well. Triangulated domain in finite number of nodes is representing the approximated unknown functions, $\boldsymbol{u}$ and η, with the interpolation between the nodes by the form functions, as follows:

$$\mathscr{V} = \left\{ \{\boldsymbol{u}, \eta\} \in [\mathscr{H}^n(\Omega)]^{\mathrm{DOF}} : \{\boldsymbol{u}, \eta\} = \text{given } \forall \boldsymbol{x} \in \partial\Omega_{\mathrm{D}} \right\}. \tag{15}$$

The Hilbertian-Sobolev space, $\mathscr{H}^n$, is of polynomial order, n, hence, we use standard Lagrange elements in the FEM [84]. On each node, we have $2+1=3$ degrees of freedom (DOFs) in two-dimensional and $3+1=4$ (DOFs) in three-dimensional spaces. As known as the Galerkin approach, the test functions, $\delta\boldsymbol{u}$ and $\delta\eta$, are approximated by the same mixed space. They vanish on Dirichlet boundaries, $\partial\Omega_{\mathrm{D}}$, where the solution, $\boldsymbol{u}$ or η, is given. For other boundaries, we use Neumann boundary condition, for displacement, $\boldsymbol{u}$, it denotes the given traction vector, $\hat{\boldsymbol{t}}$, and for twin order parameter, η, we implement zero Neumann boundaries meaning that the twin phase fails to leave the boundary across boundaries. The latter is justified easily since the twin or parent phase is neither convective nor conductive. The twin growth is inhibited by the displacement boundary conditions. The twin order parameter gradient also vanishes at the boundaries due to the Neumann boundary condition.

For time discretization, we use constant time steps in order to be able to determine an adequate time step by a convergence analysis. Given the data at a time instant, t^n, we solve $\boldsymbol{u}$ and η by a standard variational formulation leading to a weak form. The time derivative of order parameter is discretized using a so-called θ-scheme, for an arbitrary field, $y^n = y(t^n)$ and $y^{n-1} = y(t^{n-1})$, we use

$$y^{n-\theta} = (1-\theta)y^{n-1} + \theta y^{n} \,. \tag{16}$$

This scheme requires the computed solution from the last time step, y^{n-1}, by evaluating the functions within the time step, leading to a higher accuracy in the discretization [85]. For $\theta = 0$, this method is the first-order accurate explicit Euler method. For $\theta = 1$, it becomes the first-order accurate implicit Euler method. For $\theta = 0.5$, we obtain the second-order accurate Crank–Nicolson method. We use the time discretization in Eq. (14) for one finite element Ω^{e}, as follows:

$$\int_{\Omega^{\mathrm{e}}} \Bigg(\frac{\eta^{n} - \eta^{n-1}}{\Delta t} + \mathcal{L}\Big(P_{ji} F^{\mathrm{E}}_{ik} \phi'(\eta^{n-\theta}) \gamma_0 s_k m_j + 2A\eta^{n-\theta}\Big(1 - 3\eta^{n-\theta} + 2(\eta^{n-\theta})^2\Big) - 2\kappa_0 \eta^{n-\theta}_{,ii} \Big)\Bigg) \delta\eta \; \mathrm{d}V = 0 \,. \tag{17}$$

The test function, $\delta\eta$, may have a lower continuity than the trial function, η, but we stress that we aim for the Galerkin procedure such that they are chosen from the same mathematical space. In order to weaken the continuity condition on η, we integrate by parts terms of second gradient,

$$\int_{\Omega^{\mathrm{e}}} \Bigg(\frac{\eta^{n} - \eta^{n-1}}{\Delta t}\delta\eta + \mathcal{L} P_{ji} F^{\mathrm{E}}_{ik} \phi'(\eta^{n-\theta}) \gamma_0 s_k m_j \delta\eta + \mathcal{L} 2A\eta^{n-\theta}\Big(1 - 3\eta^{n-\theta} + 2(\eta^{n-\theta})^2\Big)\delta\eta + 2\mathcal{L}\kappa_0 \eta^{n-\theta}_{,i} \delta\eta_{,i} \Bigg) \; \mathrm{d}V - \int_{\partial\Omega^{\mathrm{e}}} 2\mathcal{L}\kappa_0 \eta^{n-\theta}_{,i} n_i \; \mathrm{d}A = 0. \tag{18}$$

By summing over each element, on each boundary of elements we sum twice with neighboring elements' surface normal directed oppositely. Therefore, we obtain a jump condition, which we enforce to vanish by setting it zero. In other words, the weak formulation searches for a continuous $\eta_{,i} n_i$ across element boundaries resulting in a smooth phase change within the finite element. In this way, a mesh dependency is prevented as long as the element size is adequately small such that the numerical result is converged. On the boundaries of the whole domain, we assume zero Neumann boundaries meaning that η is not leaving the domain across the outer boundary. Hence, we obtain for $\Omega = \bigcup \Omega^{\mathrm{e}}$, the following weak form:

$$\mathrm{Form}_{\eta} = \int_{\Omega} \Bigg(\frac{\eta^{n} - \eta^{n-1}}{\Delta t}\delta\eta + \mathcal{L} P_{ji} F^{\mathrm{E}}_{ik} \phi'(\eta^{n-\theta}) \gamma_0 s_k m_j \delta\eta + \mathcal{L} 2A\eta^{n-\theta}\Big(1 - 3\eta^{n-\theta} + 2(\eta^{n-\theta})^2\Big)\delta\eta + 2\mathcal{L}\kappa_0 \eta^{n-\theta}_{,i} \delta\eta_{,i} \Bigg) \; \mathrm{d}V. \tag{19}$$

Analogously, from Eq. (10), we obtain the weak form for displacement, where the traction $t_i = n_j P_{ji}$ is enforced to be continuous across the element. This so-called Newton's second lemma is a basic assumption for regular domains (no singularities). On outer boundaries, for Dirichlet boundaries, where displacement is given, the test function vanishes and we allow for Neumann boundaries that traction vector, $\hat{\boldsymbol{t}}$ in Pa, is given. The weak form for displacements, $\boldsymbol{u}$, reads

$$\mathrm{Form}_{\boldsymbol{u}} = -\int_{\Omega} P_{ji} \delta u_{i,j} \; \mathrm{d}V + \int_{\partial\Omega_{\mathrm{N}}} \hat{t}_i \delta u_i \; \mathrm{d}A \,. \tag{20}$$

The objective is to solve both fields as unknowns, $\boldsymbol{p} = \{\boldsymbol{u}, \eta\}$, at once by satisfying

$$\mathrm{Form}_{\eta} + \mathrm{Form}_{\boldsymbol{u}} = 0 \,. \tag{21}$$

The weak form is nonlinear. We use a standard Newton–Raphson linearization method, where the weak form is used to get a Jacobian by a derivative with respect to unknowns, $\boldsymbol{p}$. High-level tools are exploited to generate computer code automatically by performing a symbolic differentiation for this linearization. In this manner, use of different stored energy models is indeed possible without major changes in the implementation. We use software packages from the FEniCS Project [86,87]. The time stepping parameters are chosen such that the momentum balance scheme is second-order accurate and stable. Quadratic and linear Lagrange functions are used for the finite element approximation of the displacement and the twin order parameter, respectively. The conjugate gradient method with a Jacobi preconditioner from PETSc packages [88] has been employed for solving the nonlinear equations. The simulation has been performed by a computing node using Intel Xeon E7-4850, in total 64 cores each with the 40 MB cache, equipped with 256 GB Memory in total, running Linux Kernel 5 Ubuntu 20.04.

4 Results and discussion

The material parameters are compiled from different sources and given in Table 1. For anisotropic cases, we use the stiffness tensor with the given components and isotropic cases the Lamé constants, λ, μ. The computational domain is a 2-D rectangular shape at nanometer (nm) length-scale. Accordingly, units are chosen to be nanonewton (nN) and picosecond (ps). A mesh of 423 500 triangular elements is adopted. Initial conditions are prescribed as zero displacement and a given twin/parent phase field, which is described in each example. It is noted that 10 elements are considered at the interface to resolve the sharp variation along the interface width.

Table 1 Material properties and model constants for single crystal magnesium compiled from [16,25,69,82,89]

Parameters	Notation	Value
Second order elastic constants	$C_{11} =$	63.5 GPa
	$C_{12} =$	25.9 GPa
	$C_{13} =$	21.7 GPa
	$C_{33} =$	66.5 GPa
	$C_{44} =$	18.4 GPa
Bulk modulus	$K =$	36.9 GPa
Shear modulus	$\mu =$	19.4 GPa
Poisson's ratio	$\nu =$	0.276
Twin boundary surface energy	$\Gamma =$	0.117 J/m^2
Twinning shear for $\langle 10\bar{1}1\rangle\{\bar{1}\ 0\ 1\ 2\}$	$\gamma_0 =$	0.1295
Regularization length	$l =$	1.0 nm
Transformation barrier	$A =$	1.404 GPa
Gradient energy parameter	$\kappa_0 =$	0.0878 nJ/m
Ginzburg–Landau kinetic factor	$\mathcal{L} =$	4200(Pa s)$^{-1}$

4.1 Validation of the phase-field model and twin order parameter for single crystal magnesium

We validate our time-resolved phase-field model for single crystal magnesium using previous static phase-field results [68] and molecular dynamics simulations [69] (Fig. 1). The presence of pronounced mechanical anisotropy, local stress concentrations, and high pressure in nanoscale defect-free magnesium implies employing ansiotropic mechanical properties, anisotropic surface energy, and a large displacement formulation in our simulations. The nucleation and evolution of deformation twinning in a magnesium single crystal is simulated using the same initial twin geometry as in [68]. A circular twin embryo of initial radius $r = 3$ nm (corresponding to the analytical sharp interface solution [90]) is embedded into a rectangular domain of dimensions 40 nm $\times$ 40 nm in plane strain conditions. The $\langle 10\bar{1}1\rangle$ plane and $\{\bar{1}012\}$ directions are considered as the primary twinning system [13]. Consequently, there is no need to assume the dependency of the mobility parameter to the angle between the direction normal to the interface and a specified direction in crystal as well as temperature, due to the fact that the kinetic coefficients differ by only about 1% in different planes and directions [91]. The validation simulations in Fig. 1 are performed to investigate the twin parameter distribution subject to simple shear with Dirichlet boundary conditions on the order parameter for different cases, including an isotropic (Fig. 1(a, c, d, g, h)) and an anisotropic surface energy (Fig. 1(b, e, f, i, j)) at three different time instants. Within the simulation time of 500 ps, the twin embryo grows until it is repelled by the rigid outer boundaries. For the anisotropic case, the equilibrium shape of the twin embryo is wider in the horizontal direction (parallel to the habit plane) and flatter normal to the habit plane when compared with the isotropic case, which is in good qualitative agreement with the reference phase-field results [68] shown in Fig. 1(m). In addition, the twin interface thickness has a lower value normal to the habit plane for the anisotropic surface energy when compared with the ideal isotropic one. This may be related to the contribution of the core and elastic energies to the total surface energy of the interface [92]. For large deformation simulations (Fig. 1(b, d, f, h, j)), an orientation of the twin evolution is realized due to the difference in the driving force for twinning, which is a factor of $(\boldsymbol{F}^{\eta})^{-1}$.

Overall, the twin shape predicted by the current time-dependent phase-field approach shows features in good agreement with the molecular dynamics simulation [69] (Fig. 1(k)) and steady-state continuum-based model [68] (Fig. 1(l, m)). Finally, it is worth mentioning that the twin tends to shrink and eventually disappear when the magnitude of the shear loading was lower than $\gamma_0 = 0.07$ or the size of the initial nucleus were lower than 3 nm. This detwinning mechanism has been observed previously in copper [93] and gold nanowires [94], but this is not the focus of the present contribution.

4.2 The determination of the kinetic coefficient, $\mathcal{L}$, for magnesium using twin tip and twin boundary velocities

The kinetic coefficient or mobility parameter, $\mathcal{L}$, plays an important role in describing the twin propagation and its dependence on other parameters (e.g., shear stress) during the early stages of twin morphology [95,96]. Experimental studies lack a quantification of the twin boundary mobility in magnesium since the evolution is too fast for obtaining an adequate measurement. In order to address this, we propose to determine $\mathcal{L}$ for single crystal magnesium by

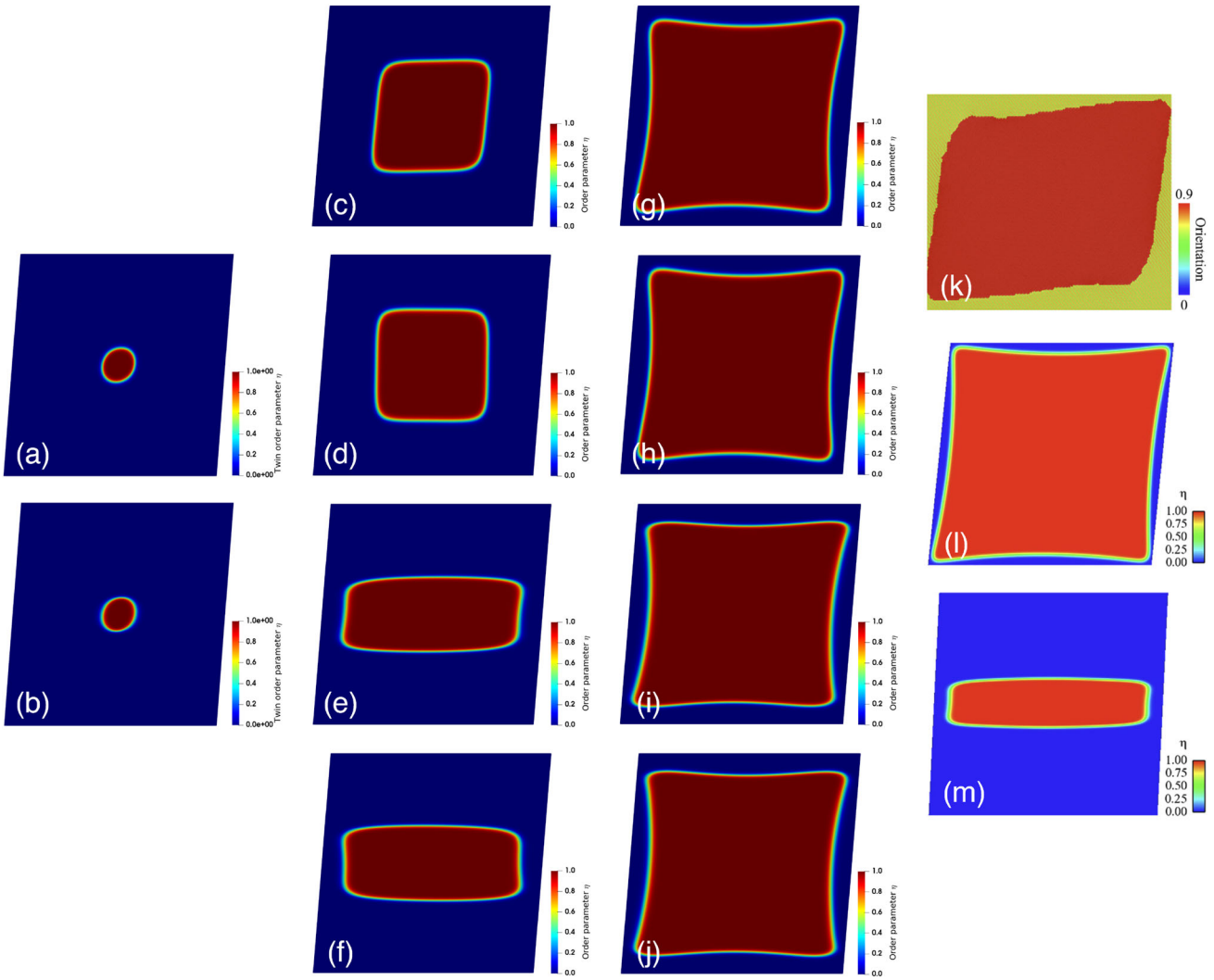

Fig. 1 Distribution of the twin order parameter, η, for an initially circular single twin with radius of 3 nm in a simple-sheared rectangular domain in both small and large deformations considering both isotropic and anisotropic surface energy and elasticity with zero orientation of the habit plane. The initial conditions are chosen to match results published in the literature using a static phase-field approach [68] and molecular dynamics model [69], while the choice of times are selected to show the evolution of the twin growth under noted conditions. (a,b) Twin order parameter for small and large strains with an isotropic surface energy at $t = 1$ ps; (c,d) Twin order parameter for small and large strains and isotropic surface energy at $t = 50$ ps; (e,f) Twin order parameter for small and large strains and anisotropic surface energy at $t = 50$ ps; (g,h) Twin order parameter for small and large strains and isotropic surface energy at $t = 500$ ps; (i,j) Twin order parameter for small and large strains and anisotropic surface energy at $t = 500$ ps; (k) Local orientation of the twinned region obtained from molecular dynamics simulations [69] and used to contrast with (g) and (h); (l,m) Order parameter for both isotropic and anisotropic surface energy under simple shear loading using a phase-field model from the literature [68], to be compared with (e) and (g). (k) and (l,m) are reproduced with permission from [68] and [69], respectively. (For interpretation of the references to color in this figure, the reader is referred to the web version of this article.)

using interface velocity profiles in both twin tip and twin boundary directions by comparing the present time-resolved phase-field results with molecular dynamics simulations [69] (Fig. 2). Here, we assume that the molecular dynamics solution represents a reliable experiment and we try to find the kinetic coefficient such that we obtain matching results. Considering a single twinning plane and direction as the primary deformation mechanism, an isotropic kinetic coefficient is obtained for predicting the microstructure evolution in two-dimensional single crystal magnesium at room temperature. This assumption is consistent with the other atomistically informed phase-field model [52,55]. Although, taking into account an anisotropic kinetic coefficient which depends on free energy functional parameters (e.g., temperature or interface orientation) is required to accurately describe the other phase transformation (e.g., liquid-liquid, liquid-vapor, and

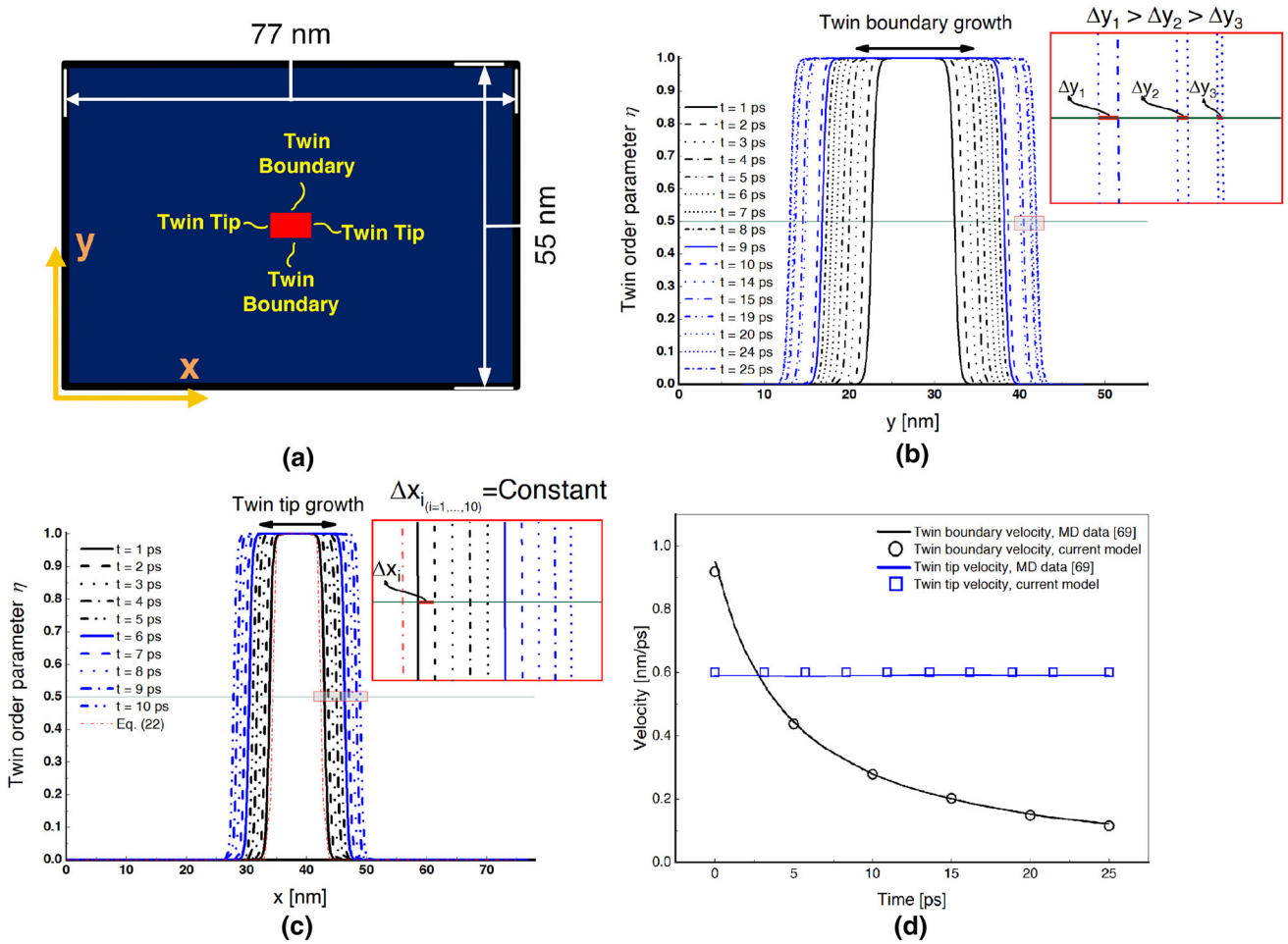

Fig. 2 Evolution of twin growth in single-crystal pure magnesium. (a) Numerical setup of the rectangular single crystal with an initial rectangular twin with boundaries and tips in material configuration; (b) Time evolution of the twin order parameter as a function of the position y normal to the habit plane. A horizontal line starting from point $\eta = 0.5$ is chosen for measuring the twin boundary interface velocity to show the interface displacement Δy. The inset demonstrates the interface profile at six different time instants to show the time-dependent growth of the twin; (c) Time evolution of the twin order parameter as a function of the position x in the direction of the habit plane. Fewer time instants than shown in (b) are used to demonstrate the constant twin tip interface velocity. Similarly, the point $\eta = 0.5$ is chosen for measuring the tip interface velocity and to show the constant interface displacement Δx. The analytical solution of the explicit Ginzburg–Landau equation, which corresponds to $t = 0$ ps, is shown as the dotted red color; (d) Twin tip and twin boundary velocities as a function of time obtained from (b) and (c), and compared with those from molecular dynamics simulations [69]. (For interpretation of the references to color in this figure, the reader is referred to the web version of this article.)

solid-melt phase transformations) interface kinetics [97]. A rectangular twin embryo with an initial length of 7 nm and width of 4.3 nm inserted at the center of a 77 nm × 55 nm rectangular domain as in Fig. 2(a). The domain is under simple-shear, the $(\bar{1}012)$ twinning planes (i.e., the horizontal planes) are referred to as twin boundaries (TB), and the $(10\bar{1}2)$ twinning planes (i.e., the vertical planes) are referred to as twin tips (TT). Applying the shear deformation in the $[10\bar{1}1]$ direction results in the twin interface profiles illustrated in Figs. 2(b) and 2(c) for the twin boundary and twin tip for times noted in the sub-figures, respectively. The twin boundary and twin tip velocities are calculated by tracking the horizontal, Δx, and vertical, Δy, interface displacement of the planes of the twin at $\eta = 0.5$ over time—along the green line in Figs. 2(b) and 2(c). The results indicate that the twin boundary (black color) and twin tip (blue color) velocities are decreasing and constant, respectively, with values of velocity summarized in Fig. 2(d). The constant velocity trend of twin tip mobility may be ascribed to the large back-stress arising at the twin tip [95]. Mapped in red onto Fig. 2(c) is the explicit analytical solution for the stationary Ginzburg–Landau equation given by [75]

$$\eta_{\text{analytical}} = \left(1 + \exp\left(\frac{-x}{w}\right)\right)^{-1}; \quad w = \sqrt{\frac{\kappa_0}{2A}}. \tag{22}$$

The comparison of numerical results with this analytical solution enables the twin interface width (i.e., difference between twin interface position at $\eta = 0.01$ and $\eta = 0.99$) to be calculated. The determination of the twin interface width is important because its size can guide the selection of the element size and spatial mesh refinement in finite element simulations of twinning [83].

Altogether, Fig. 2 provides a good validation for the present time-dependent phase-field approach, and, more importantly, enables the first ever determination of the kinetic energy coefficient, $\mathcal{L} = 4200\ (\text{Pa} \cdot \text{s})^{-1}$, for single crystal magnesium.

4.3 The time-evolved shear stress in the combined matrix-twin embryo

For a better comprehension of the underlying mechanism, we study the evolution of the twin area fraction and the shear stress, σ_{12}, in the parent and twin phase (Fig. 3). Local stress distribution within a small region in the microstructure is understood as the driving force for the propagation and growth of a twin. These insights may inform about the sequence of events leading to the formation of the visible twins at an early stage in magnesium.

In Fig. 3, the same boundary conditions and a constant 7% shear strain are used in the same rectangular twin embryo system depicted in Fig. 2(a). Initially, the length and width of a single rectangular twin embryo at different times are calculated in Fig. 3(a); this will be used to obtain the twin area fraction in Fig. 3(b). In the figure, values are calculated for $\eta = 0.5$ on the interface profile as shown in the insets at $t = 5$ ps. Results indicate that the twin growth is larger in the twin tip direction rather than in the twin boundary direction, and this difference decreases at later time instants as the twin approaches the outer boundaries.

Next, the change of the twin area fraction, defined as the ratio of the twinned to the whole simulated area, is shown in Fig. 3(b) under shear loading, and this is compared with molecular dynamics simulations [69]. The insets in Fig. 3(b) show the morphology of the twin at two different times for visualizing how the twins grow. Knowing the twin area fraction evolution is important towards enhancing our understanding of the crystal grain reorientation associated with deformation twinning, where limited data exists because of the special experimental tools needed to access the length and time scales needed to capture such measurements [27]. As seen in Fig. 3(b), the present phase-field model reasonably predicts the evolution of the twin area fraction. Next, the shear stress profile acting parallel to the x-direction is plotted for various times in Fig. 3(c), which is used to demonstrate the redistribution of internal stresses resulting from twinning [98]. The plateau and decreasing regions indicate the shear stress variation in the parent and twin phases, respectively. By progressing in time, the shear stress decreases as the x-position approaches the center of the simulation geometry, until it reaches its minimum. The magnitude of the shear stress within the twin decreases as a function of time and, eventually, becomes negative for the last time instants of the simulation. This phenomenon is consistent with experimental results [17]. At the same time, the profile evolves spatially and temporally.

Finally, the global shear stress field is shown in Fig. 3(d), where the field is taken as the average across the red line spanning both the twin and the matrix depicted in the inset. The measurements are important because they can provide insights into the complex load sharing mechanisms that are generated by the parent and the twin phase [99]. The results are also compared with molecular dynamics simulations [69], both qualitatively (the insets at $t = 10$ ps and $t = 25$ ps) and quantitatively. The phase-field results match the molecular dynamics simulations well. The results show that the global shear stress is decreasing as the twin size evolves. Altogether, results from Fig. 3 are important for determining the activation force required for twin embryo growth that may serve as an input into higher scale models [100].

4.4 Studying twin interactions toward microstructure tailoring and materials design

Finally, simulations have been performed to study the effect of twin-twin and twin-defect interactions (Fig. 4). Understanding these interactions is an important step toward developing better predictive models for designing materials with tailored properties [101–104] and microstructures [105–108]. Damage in materials is studied by phase-field models [109–113], and we use phase-field approach herein for twin interactions. These interactions [114] may result in the formation of twin-twin junctions that may cause strain hardening [115] and crack initiation [116,117], leading to a strong influence on the overall material performance. First, the change of area fraction of the middle twin as a function of time for a different number of embryos is illustrated in Fig. 4(a). Only the middle embryo is considered in the analysis in order to better isolate the interactions and reduce boundary effects. The location of the twins for the three embryo cases is illustrated in the inset. In Fig. 4(a), it is shown that increasing the number of twins leads to a decrease in the twin area fraction of the middle embryo as a result of its interaction with the other twins. The difference of the twin area fraction for multi-embryo cases becomes larger at later time instants. This finding is important as it highlights the effects of twin interactions on twin evolution, where experimental measurements are currently very limited [118]. Next, the spatial variation of the order parameter and the corresponding shear stress at $t = 10$ and $t = 20$ ps are depicted in Fig. 4(b). This result reveals insights into the expansion of

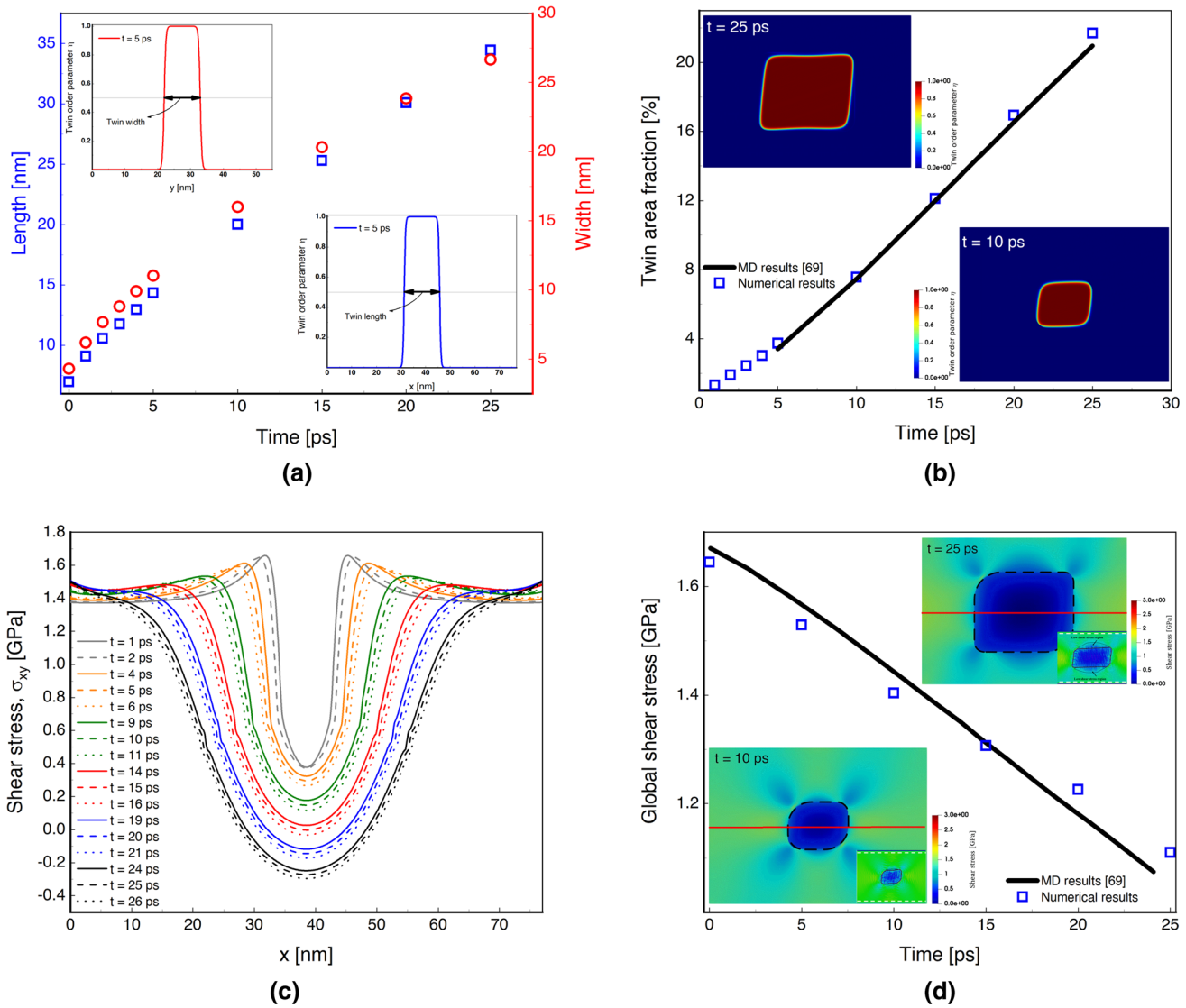

Fig. 3 The time-evolved shear stress acquired from the phase-field model on deformation twinning of single-crystal pure magnesium. (a) Time evolution of the length (blue squares) and width (red circles) of a single rectangular twin embryo that grows at 7% shear strain. The insets show the twin interface profiles at $t = 5$ ps, parallel and orthogonal to the habit plane, by which the twin size is obtained; (b) Growth of the twin area fraction (i.e., the ratio of twinned area to the total area of the numerical geometry) predicted by the proposed phase-field approach (blue squares) and compared with molecular dynamics simulations (black line) [69]. The same numerical geometry setup as [69] was used. The insets show the distribution of the twin order parameter at $t = 10$ ps and $t = 25$ ps to illustrate areal growth; (c) Spatial variation of initial shear stress along the x-axis in single-twinned magnesium at various time instants; (d) Variation of the global shear stress as a function of time. The numerical results (blue squares) are compared with molecular dynamics data (black line) [69]. The insets show the spatial distribution of local shear stress at $t = 10$ ps and $t = 25$ ps along the red mid-line. The boundaries of the twin embryo are denoted by the black dashed line. In the bottom of each insets, the atomic shear stress from snapshots taken at similar times as [69] are given for comparison. (For interpretation of the references to color in this figure, the reader is referred to the web version of this article.)

the twin domain through the accumulation of large plastic shear strain at the nano-scale [119].

The homogeneous growth in the twin area is exemplified in the top left inset in Fig. 4(b), where the twins have not changed in shape until $t = 10$ ps. The corresponding shear stress distribution at $t = 10$ ps is shown in the bottom left inset, where the shear stress inside the twins is negative while it is positive in the matrix. The heterogeneous stress distribution around the twins is due to a sudden change in the stresses within the twin interfaces, associated with the need to accommodate deformation in this region [40]. From the spatial shear stress distribution, it is observed that the local shear stress reaches a minimum in the center of each twin. Outside the twins, the shear stress is lower at the bottom

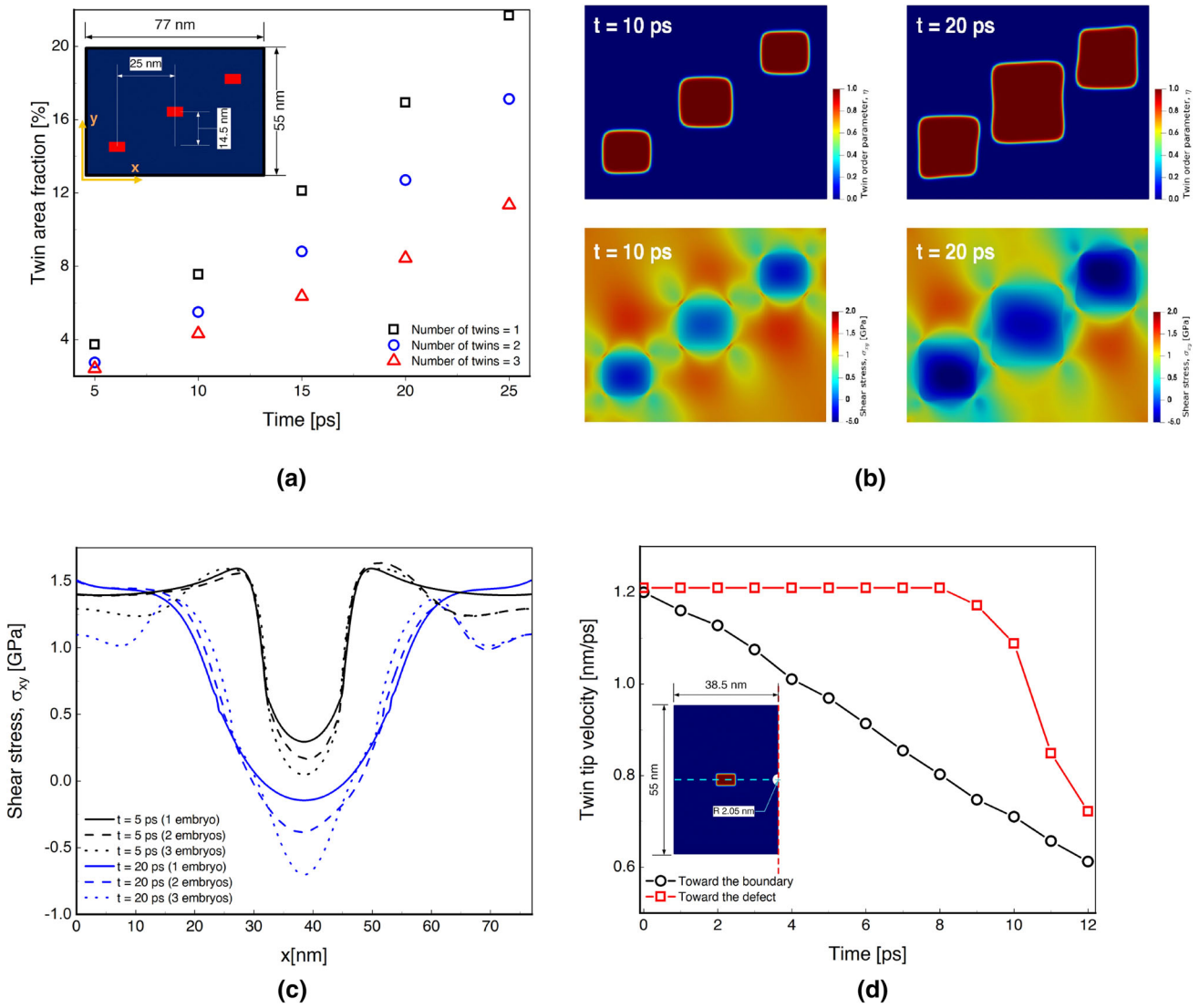

Fig. 4 Exploration of twin-twin and twin-defect interactions to inform fundamental growth mechanisms in single crystal magnesium. (a) Evolution of twin area fraction for 1, 2, and 3 twin embryos. The inset shows the location of each twin for the three-embryo simulation. The area of the middle twin is measured using its length and width obtained from the interface profile at $\eta = 0.5$, as was done for Fig. 2; (b) Spatial distribution of the twin order parameter and shear stress in the parent and twin phases for the numerical setup shown in the inset of (a) at $t = 10$ and $t = 20$ ps; (c) Evolution of the shear stress along a horizontal line through the middle of the single crystal microstructure for different numbers of embryos. The numerical setup is subjected to 7% shear strain as was done in the other examples; (d) Study of twin-defect interactions by considering the time-evolved twin tip interface towards the boundary and the void. The related simulation dimensions are given in the inset, which also shows that symmetric boundary conditions were used (the symmetry line is shown by the dash red line). (For interpretation of the references to color in this figure, the reader is referred to the web version of this article.)

left and top right twins because of the constraining effect of the adjacent twins to the middle one. In the right insets, the deviatoric deformation in twin morphology at $t = 20$ ps is identified due to the interaction of the twins with each other and the disturbing of the stress field by them. The stress distribution in the vicinity of the twin-matrix interfaces at $t = 20$ ps is heterogeneous as a result of high stress concentrations in the matrix near the twin boundaries. It is also shown that the middle twin experiences a maximum shear stress resulting from the compressive forces generated by the other twins. The local stress concentration is one main interaction of crack and twins where some nucleation site appears in the interfaces inside and around the interface [120].

Next, the change of shear stress along a horizontal line through a middle section of the simulation area as a function of a 1, 2, or 3 embryo system is shown in Fig. 4(c). It is observed that increasing the number of twins leads to decreasing the shear stress values in the matrix phase,

while the difference in shear stress values for the later time instants are larger as a result of twin-twin interactions. In the twinned regions at later times, the junctions of different embryos result in a negative shear stress with steeper slopes as compared with earlier times. In addition, it can be observed that the stress concentration in the matrix, predominantly in the vicinity of the twin boundaries, increases only marginally with increasing twin thickness (black lines in Fig. 4(c)). Finally, the interaction of a twin and a defect is investigated in Fig. 4(d) by comparing the change in the twin tip velocity towards the boundary and the void along the blue dashed horizontal line. The numerical setup is also given in the inset, where symmetric boundary conditions are used. The radius of 2 nm is chosen for the void. For all times, the results indicate that the tip velocity is linearly decreasing in time in a direction approaching the left boundary. For the void, the velocity at the tip is constant until some point after which a sudden decrease in the velocity occurs, resulting from the twin-defect interaction. In addition, the twin tip velocity is larger toward the void because of the higher stress concentration influenced by the void.

5 Conclusions

In this paper, the evolution of twinning in magnesium has been studied using a validated and calibrated phase-field model to gain better insights into the time-evolved twin morphology, the spatial distribution of the internal shear stress, and the twin interactions. An accurate monolithic iterative procedure has been implemented for solving the coupled balance and Ginzburg–Landau equations, and the governing equations have been solved in the open-source high-level computing platform, FEniCS. For engineering examples with FEniCS, we refer to [121].

The results presented in this work confirmed the impact of the current model by capturing the behavior of the leading deformation mechanism in single crystal magnesium, twinning. By means of the proposed implementation, the state variables (i.e., the displacement and the twin order parameter) have been computed monolithically for various scenarios in discrete time steps, including small and large deformations with both isotropic and anisotropic surface energies and elasticity. The data have been compared with a continuum mechanics model [68] and molecular dynamics simulations [69]. The findings are qualitatively consistent with both literature approaches.

A notable result emerging from the proposed model is the prediction of the critical strain and initial twin embryo size required for growth and propagation under the chosen numerical settings. This computational implementation is particularly useful because identifying such features experimentally is challenging given the length and time scales needed to reproduce these events [122]. Next, the interface velocities for the twin tips and twin boundaries have been explored in order to determine the kinetic coefficient using the phase-field model and compared with recent molecular dynamics simulation [69]. Studying velocity growths is important because they affect hardening, texture evolution, and ductility in the material [123]. To the authors' best knowledge, the present work pioneers the analysis of the interface mobility, showing different trends of twin evolution in the direction parallel and orthogonal to the twin habit plane.

The interface velocity is considered to be an important factor to determine the thermodynamic driving force for interface propagation, because knowing the interface velocity for any value of the driving force potentially leads to the determination of the kinetic coefficient for any range of materials [124]. The interface profile has been compared with the analytical solution of the stationary Ginzburg–Landau equation, and the obtained numerical interface width of 1.58 nm is close to the analytical value of 1.62 nm [75]. This information guides mesh selection and refinement when modeling twinning in this system [125, 126]. In addition, the current phase-field modeling approach overcomes the challenges existing in molecular dynamic simulations for calculating the twin size, such as identifying the orientation of each atom in the twinned region [36], and is able to capture new behavior of twin growth for $t \leq 5$ ps, comparing well with previous molecular dynamics data [69]. The strong point of the current approach is to track multiple interfaces in order to measure twins' size with no additional efforts for samples larger or smaller than in atomistic simulations.

A further considerable implication of the proposed model is the possibility of investigating the local and global shear stress field inside the parent and twinned phases. Analysis of twin shear stress fields induced in these cases provides further evidence for the effect of twins' thickness and their mutual position on further twin growth and/or further twin nucleation [127–129]. Moreover, the importance of an appropriate strategy for partitioning the stress fields between the twinned and untwinned domains have been demonstrated in this paper. A final upshot of the current phase-field model has been to explore new understandings in twin-twin and twin-defect interactions. For the case where multiple twins grow in one grain, a common occurrence observed in experiments [130], it is highlighted that the stress concentration around the void may significantly increase the twin interface velocity, affecting subsequent expansion of the twins. Taken together, our study provides a framework for a new way to understand local deformation mechanisms in materials by analyzing the evolution and interaction of twins.

Acknowledgements The authors acknowledge support from Natural Sciences and Engineering Research Council of Canada (NSERC) Discovery Grant 2016-04685 and NSERC DNDPJ 531130-18,U.S. Army

Research Laboratory funding (W911NF-17-2-0213), and partial support of the MIUR-PRIN project XFAST-SIMS (no. 20173C478N).

Funding Open access funding provided by Uppsala University.

Data Availability The authors declare that the main data supporting the findings of this study are available within this article. Extra data are available from the corresponding authors upon reasonable request.

Code availability The Python code, generated during the current study, is part of the FEniCS project available at http://www.fenicsproject.org/download, and an example for the computational implementation is available in [131] to be used under the GNU Public license [132].

Declaration of competing interests The authors declare no competing financial interests or personal relationships.

CRediT Authorship Contributions Statement B.A developed the model, wrote the code, designed and performed all simulations, analyzed results, and wrote the original draft. H.J analyzed results, reviewed, and edited the paper. B.E.A developed the model and the code, allocated the computational resources, reviewed and edited the paper. A.R helped in computational aspects, reviewed and edited the paper. J.D.H supervised the research, acquired funding, reviewed, and edited the paper. All authors discussed the results.

References

1. Chen M, Ma E, Hemker KJ, Sheng H, Wang Y, Cheng X (2003) Deformation twinning in nanocrystalline Alum. Sci 300(5623): 1275–1277
2. (2010) Strong crystal size effect on deformation twinning. Nature 463(7279):335–338
3. Chen G, Peng Y, Zheng G, Qi Z, Wang M, Yu H, Dong C, Liu C (2016) Polysynthetic twinned tial single crystals for high-temperature applications. Nature Mater 15(8):876–881
4. Hirsch J, Al-Samman T (2013) Superior light metals by texture engineering: Optimized aluminum and magnesium alloys for automotive applications. Acta Mater 61(3): 818–843.The Diamond Jubilee Issue
5. Liao X, Zhao Y, Srinivasan S, Zhu Y, Valiev R, Gunderov D (2004) Deformation twinning in nanocrystalline copper at room temperature and low strain rate. App Phy Letter 84(4):592–594
6. Zhang X, Wu X, Zhu A (2009) Growth of deformation twins in room-temperature rolled nanocrystalline nickel. App Phy Letter. 94(12): 121907
7. McCabe RJ, Proust G, Cerreta EK, Misra A (2009) Quantitative analysis of deformation twinning in zirconium. Int J Plast 25(3): 454–472
8. McCabe R, Capolungo L, Marshall P, Cady C, Tomé C (2010) Deformation of wrought uranium: Experiments and modeling. Acta Mater 58(16): 5447–5459
9. Guo T, Chao Q, Siska F, Cheng J, Varma RR, Barnett MR (2018) Analysing single twinning events in Mg-6Zn using nanoindentation. J Alloy Compd 768: 510–516
10. Wu Z, Ahmad R, Yin B, Sandlöbes S, Curtin W(2018) Mechanistic origin and prediction of enhanced ductility in magnesium alloys. Sci 359(6374):447
11. Joost WJ, Krajewski PE (2017) Towards magnesium alloys for high-volume automotive applications. Scripta Mater 128:107–112
12. Wang J, Wang X, Yu K, Rupert TJ, Mahajan S, Lavernia EJ, Schoenung JM, Beyerlein IJ (2021) Manipulating deformation mechanisms with y alloying of mg. Mater Sci Eng: A 817:141,373
13. Staroselsky A, Anand L (2003) A constitutive model for hcp materials deforming by slip and twinning: application to magnesium alloy az31b. Int J Plast 19(10):1843–1864
14. Lentz M, Klaus M, Beyerlein IJ, Zecevic M, Reimers W, Knezevic M (2015) In situ X-ray diffraction and crystal plasticity modeling of the deformation behavior of extruded Mg-Li-(Al) alloys: An uncommon tension-compression asymmetry. Acta Mater 86:254–268
15. Capolungo L, Beyerlein I, Tomé C (2009) Slip-assisted twin growth in hexagonal close-packed metals. Scr Mater 60(1): 32–35
16. Christian J, Mahajan S (1995) Deformation twinning. Prog Mater Sci 39(1): 1–157
17. ArulKumar M (2018) Deformation twinning and grain partitioning in a hexagonal close-packed magnesium alloy. Nature Commun 9(1):4761
18. Leu B, Kumar MA, Beyerlein IJ (2021) The effects of free surfaces on deformation twinning in hcp metals. Mater 17(101):124
19. Yang F, Yin S, Li S, Zhang Z (2008) Crack initiation mechanism of extruded AZ31 magnesium alloy in the very high cycle fatigue regime. Materials Science and Engineering: A 491(1): 131–136
20. Tang J, Tian X, Jiang W, Wang Q, Wei D, Zhang X, Fan H (2021) Interactions between twin boundary and point defects in magnesium at low temperature. J. Mater Res pp. 1–12
21. Abdolvand H, Wright J, Wilkinson AJ (2018) Strong grain neighbour effects in polycrystals. Nature Communications 9(1):171
22. Zhao X, Chen H, Wilson N, Liu Q, Nie JF (2019) Direct observation and impact of co-segregated atoms in magnesium having multiple alloying elements. Nature Communications 10(1):3243
23. Fan H, Zhu Y, El-Awady JA, Raabe D (2018) Precipitation hardening effects on extension twinning in magnesium alloys. Int J. Plast 106:186–202
24. Hu Y, Turlo V, Beyerlein IJ, Mahajan S, Lavernia EJ, Schoenung JM, Rupert TJ (2020) Embracing the chaos: Alloying adds stochasticity to twin embryo growth. Phys. Rev. Lett. 125(205):503
25. Wang J, HirthJP, Tomé CN (2009) $(\bar{1}012)$ twinning nucleation mechanisms in hexagonal-close-packed crystals. Acta Materialia 57(18): 5521–5530
26. Cao Y, Zhang L, Y. Zhang Y (2016) Twinning interactions induced amorphisation in ultrafine silicon grains. Mater Sci Eng: A 658:321–325
27. Kannan V, Hazeli K, Ramesh K (2018) The mechanics of dynamic twinning in single crystal magnesium. J Mech Phy Solids 120:154–178
28. Beyerlein I, Capolungo L, Marshall P, McCabe R, Tomé C (2010) Statistical analyses of deformation twinning in magnesium.Philos Mag 90(16): 2161–2190
29. Li B, Ma E (2009) Atomic shuffling dominated mechanism for deformation twinning in magnesium. Phys. Rev. Lett. 103(035):503

30. Hirth J, Wang J, Tomé C (2016) Disconnections and other defects associated with twin interfaces. Progs Mater Sci 83:417–471
31. Zhang J, Xi G, Wan X, Fang C (2017) The dislocation-twin interaction and evolution of twin boundary in AZ31 Mg alloy. Acta Materialia 133:208–216
32. Wu Z, Francis M, Curtin W (2014) Magnesium interatomic potential for simulating plasticity and fracture phenomena. Model Simul Mater Sci Eng 23(1):015004
33. Benzerga A, Thomas N, Herrington JS (2019) Plastic flow anisotropy drives shear fracture. Sci Reports 9(1):1425
34. Kelchner CL, Plimpton S, Hamilton J (1998) Dislocation nucleation and defect structure during surface indentation. Phys. Rev. B 58(11):085–11088
35. Ackland GJ, Jones AP (2006) Applications of local crystal structure measures in experiment and simulation. Phys. Rev. B 73(054):104
36. Agarwal G, Dongare AM (2019) Deformation twinning in polycrystalline Mg microstructures at high strain rates at the atomic scales. Scientific Reports 9(1):3550
37. Glüge R, Bertram A, Böhlke T, Specht E (2010) A pseudoelastic model for mechanical twinning on the microscale. ZAMM - J App Math Mech / Z Angew Math Mech 90(7-8): 565–594
38. Cheng J, Ghosh S (2015) A crystal plasticity FE model for deformation with twin nucleation in magnesium alloys. Int J Plast 67:148–170 doi10.1016/j.ijplas.2014.10.005
39. Kolupaev V, Yu MH, Altenbach H (2013) Yield criteria of hexagonal symmetry in the π-plane. Acta Mech 224(7):1527–1540
40. Liu C, Shanthraj P, Diehl M, Roters F, Dong S, Dong J, Ding W, Raabe D (2018) An integrated crystal plasticity-phase field model for spatially resolved twin nucleation, propagation, and growth in hexagonal materials. Int J Plast 106:203–227
41. Kondo R, Tadano Y, Shizawa K (2014) A phase-field model of twinning and detwinning coupled with dislocation-based crystal plasticity for hcp metals. Comput Mater Sci 95:672–683
42. Li Y, Hu S, Barker E, Overman N, Whalen S, Mathaudhu S (2020) Effect of grain structure and strain rate on dynamic recrystallization and deformation behavior: A phase field-crystal plasticity model. Comput Mater Sci 180(109):707
43. Levitas VI (2018) Phase field approach for stress-and temperature-induced phase transformations that satisfies lattice instability conditions. part i. general theory. Int J Plast 106:164–185
44. Chen LQ (2002) Phase-field models for microstructure evolution. Ann Rev Mater Res 32(1):113–140
45. Hirshikesh H, Pramod A, Waisman H, Natarajan S (2021) Adaptive phase field method using novel physics based refinement criteria. Comput Meth App Mech Eng 383(113):874
46. Yi LP, Waisman H, Yang ZZ, Li XG (2020) A consistent phase field model for hydraulic fracture propagation in poroelastic media. Comput Meth App Mech Eng 372(113):396
47. Hansen-Dörr AC, Dammaß F, de Borst R, Kästner M (2020) Phase-field modeling of crack branching and deflection in heterogeneous media. Eng Fract Mech 232(107):004
48. Liu C, Shanthraj P, Diehl M, Roters F, Dong S, Dong J, Ding W, Raabe D (2018) An integrated crystal plasticity-phase field model for spatially resolved twin nucleation, propagation, and growth in hexagonal materials. Int J Plast 106:203–227
49. Pi Z, Fang Q, Liu B, Feng H, Liu Y, Liu Y, Wen P (2016) A phase field study focuses on the transverse propagation of deformation twinning for hexagonal-closed packed crystals. Int J Plast 76:130–146
50. Hu X, Ji Y, Heo TW, Chen LQ, Cui X (2020) Phase-field model of deformation twin-grain boundary interactions in hexagonal systems. Acta Mater 200:821–834
51. Hu X, Ji Y, Chen L, Lebensohn RA, Chen LQ, Cui X (2021) Spectral phase-field model of deformation twinning and plastic deformation. Int. J. Plast 143(103):019
52. Ishii A (2020) Energetics of heterogeneous Mg $\{10\bar{1}2\}$ deformation twinning migration using an atomistically informed phase-field model. Comput. Mater Sci 183(109):907
53. Chen LQ, Shen J (1998) Applications of semi-implicit fourier-spectral method to phase field equations. Comput Phy Commun 108(2–3):147–158
54. Levin VA, Levitas VI, Zingerman KM, Freiman EI (2013) Phase-field simulation of stress-induced martensitic phase transformations at large strains. Int J Solid Struct 50(19):2914–2928
55. Gong M, Graham J, Taupin V, Capolungo L (2021) The effects of stress, temperature and facet structure on growth of $\{10\bar{1}2\}$ twins in Mg: A molecular dynamics and phase field study. Acta Mater 208(116):603
56. Ma R, Sun W (2021) Phase field modeling of coupled crystal plasticity and deformation twinning in polycrystals with monolithic and splitting solvers. Int J Numer Meth Eng 122(4):1167–1189
57. Kumar MA, Kanjarla A, Niezgoda S, Lebensohn R, Tomé C (2015) Numerical study of the stress state of a deformation twin in magnesium. Acta Mater 84:349–358
58. Bhattacharya K (2003) Microstructure of martensite: why it forms and how it gives rise to the shape-memory effect. Oxford Series on Materials Modelling, vol. 2. Oxford University Press
59. Grilli N, Cocks AC, Tarleton E (2020) A phase field model for the growth and characteristic thickness of deformation-induced twins. J Mech Phy Solid 143(104):061
60. Liu G, Mo H, Wang J, Shen Y (2021) Coupled crystal plasticity finite element-phase field model with kinetics-controlled twinning mechanism for hexagonal metals. Acta Mater 202:399–416
61. Clayton J, Knap J (2016) Phase field modeling and simulation of coupled fracture and twinning in single crystals and polycrystals. Comput Meth App Mech Eng 312:447–467
62. Zhang RY, Daymond MR, Holt RA (2011) Parametric study of stress state development during twinning using 3d finite element modeling. Materials Science and Engineering: A 528(6): 2725–2735
63. Arul Kumar M, Beyerlein I, Tomé C (2016) Effect of local stress fields on twin characteristics in hcp metals. Acta Mater 116:143–154
64. Schreiber C, Kuhn C, Müller R, Zohdi T (2020) A phase field modeling approach of cyclic fatigue crack growth. Int J Fract 225(1):89–100
65. Schlüter A, Willenbücher A, Kuhn C, Müller R (2014) Phase field approximation of dynamic brittle fracture. Comput Mech 54(5):1141–1161
66. Hansen-Dörr AC, de Borst R, Hennig P, Kästner M (2019) Phase-field modelling of interface failure in brittle materials. Comput Meth App Mech Eng 346:25–42
67. Rosakis P, Tsai H (1995) Dynamic twinning processes in crystals. Int J Solid Struct 32(17–18):2711–2723
68. Clayton J, Knap J (2011) A phase field model of deformation twinning: Nonlinear theory and numerical simulations. Phy D: Nonlinear Phenom 240(9): 841–858
69. Hu Y, Turlo V, Beyerlein IJ, Mahajan S, Lavernia EJ, Schoenung JM, Rupert TJ (2020) Disconnection-mediated twin embryo growth in mg. Acta Mater 194:437–451
70. Lyulin AV, Balabaev NK, Mazo MA, Michels M (2004) Molecular dynamics simulation of uniaxial deformation of glassy amorphous atactic polystyrene. Macromol 37(23):8785–8793
71. Park H, Choi J, Kim B, Yang S, Shin H, Cho M (2018) Toward the constitutive modeling of epoxy matrix: Temperature-accelerated quasi-static molecular simulations consistent with the experimental test. Comp Part B: Eng 142:131–141
72. Rice JR (1971) Inelastic constitutive relations for solids: an internal-variable theory and its application to metal plasticity. J Mech Phy Solid 19(6):433–455

73. Yagyu H (2015) Coarse-grained molecular dynamics simulation of the effects of strain rate on tensile stress of cross-linked rubber. Soft Mater 13(4):263–270
74. Struleva EV, Komarov PS, Ashitkov SI (2019) Dynamic strength of titanium melt at extremely high extension rates. High Temp 57(6):948–950
75. Farrahi GH, Javanbakht M, Jafarzadeh H (2020) On the phase field modeling of crack growth and analytical treatment on the parameters. Cont Mech Thermo 32(3):589–606
76. Farbaniec L, Williams C, Kecskes L, Becker R, Ramesh K (2017) Spall response and failure mechanisms associated with a hot-extruded amx602 mg alloy. Mater Sci Eng: A 707:725–731
77. James RD (1981) Finite deformation by mechanical twinning. Arch Ration Mech Anal 77(2):143–176
78. Levitas VI, Preston DL (2002) Three-dimensional landau theory for multivariant stress-induced martensitic phase transformations. i. austenite↔martensite. Phys. Rev. B 66, 134,206
79. Levitas VI, Preston DL (2005) Thermomechanical lattice instability and phase field theory of martensitic phase transformations, twinning and dislocations at large strains. Phy Lett A 343(1): 32–39
80. Hill R (1952) The elastic behaviour of a crystalline aggregate. Proc. Phy Soc. Sect A. 65(5):349
81. Clayton J (2009) A continuum description of nonlinear elasticity, slip and twinning, with application to sapphire. Proceedings of the Royal Society A: Math, Phy Eng Sci 465(2101):307–334
82. Levitas VI (2009) Displacive phase transitions at large strains: Phase-field theory and simulations. Phys. Rev. Lett. 103(025):702
83. Levitas VI (2014) Phase field approach to martensitic phase transformations with large strains and interface stresses. J Mech Phy Solid 70:154–189
84. Zohdi TI (2018) Finite element primer for beginners. Springer
85. Chung J, Hulbert G (1993) A time integration algorithm for structural dynamics with improved numerical dissipation: the generalized-α method
86. Logg A, Wells GN (2010) Dolfin: Automated finite element computing. ACM Trans. Math. Softw. 37(2) doi:114sps5/1731022.1731030
87. Ølgaard KB, Logg A, Wells GN (2009) Automated code generation for discontinuous galerkin methods. SIAM Journal on Scientific Computing 31(2):849–864
88. Balay S, Abhyankar S, Adams MF, Brown J, Brune P, Buschelman K, Dalcin L, Dener A, Eijkhout V, Gropp WD, Karpeyev D, Kaushik D, Knepley MG, May DA, McInnes LC, Mills RT, Munson T, Rupp K, Sanan P, Smith BF, Zampini S, Zhang H, Zhang H (2021) PETSc users manual. Tech. Rep. ANL-95/11 - Revision 3.15, Argonne National Laboratory
89. Slutsky LJ, Garland CW (1957) Elastic constants of magnesium from 4.2°K to 300°K. Phys. Rev. 107:972–976
90. Lee J, Yoo M (1990) Elastic strain energy of deformation twinning in tetragonal crystals. Metall Trans A 21(9):2521–2530
91. Kavousi S, Novak BR, Zaeem BR, Moldovan D (2019) Combined molecular dynamics and phase field simulation investigations of crystal-melt interfacial properties and dendritic solidification of highly undercooled titanium. Comput Mater Sci 163:218–229
92. Kosevich AM, Bouko VS (1971) Dislocation theory of the elastic twinning of crystals. Soviet Physics Uspekhi 14(3):286–316
93. Wang J, Li N, Anderoglu O, Zhang X, Misra A, Huang J, J. Hirth, (2010) Detwinning mechanisms for growth twins in face-centered cubic metals. Acta Materialia 58(6): 2262–2270
94. Lee S, Im J, Yoo Y, Bitzek E, Kiener D, Richter G, Kim B, Oh SH (2014) Reversible cyclic deformation mechanism of gold nanowires by twinning-detwinning transition evidenced from in situ tem. Nature Commu 5(1):1–10
95. Máthis K et al (2021) On the dynamics of twinning in magnesium micropillars. Materials & Design 203:109,563
96. Morrow B, Cerreta E, McCabe R, Tomé C (2014) Toward understanding twin-twin interactions in hcp metals: Utilizing multiscale techniques to characterize deformation mechanisms in magnesium. Mater Sci Eng: A 613:365–371
97. Bergmann S, Albe K, Flegel E, Barragan-Yani D, Wagner B (2017) Anisotropic solid–liquid interface kinetics in silicon: an atomistically informed phase-field model. Modelling and Simulation in Materials Science and Engineering 25(6): 065,015
98. Clausen B, Tomé C, Brown D, Agnew S (2008) Reorientation and stress relaxation due to twinning: Modeling and experimental characterization for mg. Acta Mater 56(11):2456–2468
99. Mareau C, Daymond MR (2016) Micromechanical modelling of twinning in polycrystalline materials: Application to magnesium. Int J Plast 85:156–171
100. Hürkamp A, Gellrich S, Ossowski T, Beuscher J, Thiede S, Herrmann C, Dröder K (2020) Combining simulation and machine learning as digital twin for the manufacturing of overmolded thermoplastic composites. J Manuf Mater Proc 4(3):92
101. dell'Isola F, Steigmann DJ (2020) *Discrete and Continuum Models for Complex Metamaterials* (Cambridge University Press)
102. Giorgio I, Ciallella A, Scerrato D (2020) A study about the impact of the topological arrangement of fibers on fiber-reinforced composites: some guidelines aiming at the development of new ultra-stiff and ultra-soft metamaterials. Int J Solid Struct 203:73–83
103. Barchiesi E, Spagnuolo M, Placidi L (2019) Mechanical metamaterials: a state of the art. Math Mech Solid 24(1):212–234
104. Hu JM, Duan CG, Nan CW, Chen LQ (2017) Understanding and designing magnetoelectric heterostructures guided by computation: progresses, remaining questions, and perspectives. npj Comput Mater 3(1): 1–21
105. dell'Isola F, WoŹniak, (1997) On phase transition layers in certain micro-damaged two-phase solids. International Journal of Fracture 83(2):175–189
106. Aldakheel F (2020) A microscale model for concrete failure in poro-elasto-plastic media. Theor App Fract Mech 107(102):517
107. Madeo A, Corte AD, Giorgio I, Scerrato D (2017) Modeling and designing micro-and nano-structured metamaterials: towards the application of exotic behaviors. Math Mech Solid 22(4):873–884
108. Temizer I, Wriggers P (2010) A micromechanically motivated higher-order continuum formulation of linear thermal conduction. ZAMM-J App Math Mech/Z Angew Math Mech 90(10–11):768–782
109. Cottura M, Le Bouar Y, Finel A, Appolaire B, Ammar K, Forest S (2012) A phase field model incorporating strain gradient viscoplasticity: application to rafting in ni-base superalloys. J Mech Phy Solid 60(7):1243–1256
110. Aldakheel F (2016) Mechanics of nonlocal dissipative solids: gradient plasticity and phase field modeling of ductile fracture (Stuttgart: Institut für Mechanik (Bauwesen). Universität Stuttgart), Lehrstuhl I
111. Placidi L, Barchiesi E, Misra A (2018) A strain gradient variational approach to damage: a comparison with damage gradient models and numerical results. Math Mech Complex Syst 6(2):77–100
112. Dammaß F, Ambati M, Kästner M (2021) A unified phase-field model of fracture in viscoelastic materials. Cont Mech Thermody pp. 1–23
113. Abali BE, Klunker A, Barchiesi E, Placidi L (2021) A novel phase-field approach to brittle damage mechanics of gradient metamaterials combining action formalism and history variable. ZAMM-J App Math Mech/Z Angew Math Mech p. e202000289
114. Forest S, Parisot R (2000) Material crystal plasticity and deformation twinning. Rendiconti del Seminario Matematico dell'Universita e del Politec di Torino 58:99–111

115. Sun Q, Ostapovets A, Zhang X, Tan L, Liu Q (2018) Investigation of twin-twin interaction in deformed magnesium alloy. Philos Mag 98(9):741–751
116. Sim GD, Kim G, Lavenstein S, Hamza MH, Fan H, El-Awady JA (2018) Anomalous hardening in magnesium driven by a size-dependent transition in deformation modes. Acta Mater 144:11–20
117. Yeratapally SR, Glavicic MG, Hardy M, Sangid MD (2016) Microstructure based fatigue life prediction framework for polycrystalline nickel-base superalloys with emphasis on the role played by twin boundaries in crack initiation. Acta Materialia 107:152–167
118. Bönisch M, Wu Y, Sehitoglu H (2018) Hardening by slip-twin and twin-twin interactions in femnnicocr. Acta Materialia 153:391–403
119. Cheng J, Ghosh S (2017) Crystal plasticity finite element modeling of discrete twin evolution in polycrystalline magnesium. J Mech Phy Solid 99:512–538
120. Jafarzadeh H, Levitas VI, Farrahi GH, Javanbakht M (2019) Phase field approach for nanoscale interactions between crack propagation and phase transformation. Nanoscale 11:22,243–22,247
121. Abali BE (2017) Computational Reality, Advanced Structured Materials, vol 55. Springer Nature, Singapore
122. Liu Y, Li N, Arul Kumar M, Pathak S, Wang J, McCabe R, Mara N, Tomé C (2017) Experimentally quantifying critical stresses associated with basal slip and twinning in magnesium using micropillars. Acta Mater 135:411–421
123. Gong M, Liu G, Wang J, Capolungo L, Tomé CN (2018) Atomistic simulations of interaction between basal $<a>$ dislocations and three-dimensional twins in magnesium. Acta Mater 155:187–198
124. Levitas VI (2013) Phase-field theory for martensitic phase transformations at large strains. Int J Plast 49:85–118
125. Momeni K, Levitas VI (2015) A phase-field approach to solid-solid phase transformations via intermediate interfacial phases under stress tensor. Int J Solid Struct 71:39–56
126. Amirian B, Jafarzadeh H, Abali BE, Reali A, Hogan JD (2022) Thermodynamically-consistent derivation and computation of twinning and fracture in brittle materials by means of phase-field approaches in the finite element method. Int J Solids Struct 252:111789
127. Robson J (2016) The effect of internal stresses due to precipitates on twin growth in magnesium. Acta Mater 121:277–287
128. Jang D, Li X, Gao H, Greer JR (2012) Deformation mechanisms in nanotwinned metal nanopillars. Nature nanotechnology 7(9):594
129. Hutchinson W, Barnett M (2010) Effective values of critical resolved shear stress for slip in polycrystalline magnesium and other hcp metals. Scripta Materialia 63(7): 737–740
130. Jung J, Yoon JI, Kim JG, Latypov MI, Kim JY, Kim HS (2017) Continuum understanding of twin formation near grain boundaries of fcc metals with low stacking fault energy. npj Comput Mater 3(1): 1–9
131. Abali BE (2020) Supply code for computations. http://bilenemek.abali.org/
132. GNU Public. Gnu general public license (2007). http://www.gnu.org/copyleft/gpl.html